Formation of Carbon Nanofibers and Carbon Nanotubes through Methane Decomposition over Supported Cobalt Catalysts

Sakae Takenaka,*,† Minoru Ishida,† Michio Serizawa,† Eishi Tanabe,‡ and Kiyoshi Otsuka*,†

Department of Applied Chemistry, Graduate School of Science and Engineering, Tokyo Institute of Technology, 2-12-1 Ookayama, Meguro-ku, Tokyo 152-8552, Japan, and Western Hiroshima Prefecture Industrial Institute, Kagamiyama, Higashi-Hiroshima, Hiroshima 739-0046, Japan

Received: March 16, 2004; In Final Form: April 30, 2004

Catalytic performance of Co catalysts supported on different supports (MgO, Al_2O_3, SiO_2, and TiO_2) for the formation of carbon nanofibers through methane decomposition was investigated. Catalytic activity and the life of supported Co catalysts for methane decomposition at 773 K strongly depended on the type of catalytic supports; i.e., the catalytic performances of Co/Al_2O_3 and Co/MgO were superior to those of Co/TiO_2 and Co/SiO_2. All the Co catalysts produced carbon nanofibers with relatively uniform diameters (10−30 nm) through the reaction at 773 K irrespective of the kind of catalytic supports, although an average crystallite size of Co metal was different for these catalysts. These results implied that Co metal particles with diameters from 10 to 30 nm grew carbon nanofibers from methane preferentially, while ones larger than 30 nm were inactive for the reaction. The structures of carbons formed by methane decomposition over Co/Al_2O_3 depended on the reaction temperatures. Multiwalled carbon nanotubes (MWCNT) were produced mainly in the temperature range of 873−973 K, where the catalytically active Co metal particles were present at the tip or in the hollow of MWCNT. On the other hand, helically coiled carbon nanotubes and bamboolike carbon nanotubes were formed preferentially at 1073 K, where Co metal particles could be rarely observed in the carbons. These results implied that the growth mechanisms of these carbons by Co metal particles were changed according to the reaction temperatures. Co K-edge XANES and EXAFS suggested that Co species on the supported Co catalysts were always present as Co metal during the methane decomposition, irrespective of the kinds of catalytic supports or the reaction temperatures.

1. Introduction

Carbon nanofibers and carbon nanotubes have attracted a great deal of interest since the discovery of carbon nanotubes.[1] These nanoscale carbon materials are expected to have a variety of applications for hydrogen storage, chemical sensor, catalytic supports, field emitters in the display, and so on, because they have remarkable and unique magnetic, electronic, chemical, and mechanical properties.[2−4] The preparation of nanoscale carbon materials usually requires severe reaction conditions such as high temperatures. For example, single-walled carbon nanotubes (SWCNT) and multiwalled carbon nanotubes (MWCNT) are synthesized by the carbon arc discharge process and the laser ablation of graphite elecrodes.[5,6] These methods can produce SWCNT or MWCNT with relatively high selectivity. However, these methods are not adequate for the mass production of nanoscale carbon materials, since they require a large energy input and cannot supply continuously carbon sources for the carbon nanotubes.

Catalytic decomposition of molecules containing carbon atoms such as CO and hydrocarbons (CVD; chemical vapor deposition) is the promising method for the production of nanoscale carbon materials at lower costs with larger scales.[7−9] The structures of nanoscale carbons formed by this method strongly depend on the kind of molecules for their carbon sources as well as the type of metal catalysts.[10−12] Ni catalysts have been frequently used for the synthesis of carbon nanofibers without a hollow structure through the decomposition of hydrocarbons.[13−16] Supported Ni catalysts are one of the catalysts with the highest activity and the longest life for the decomposition of hydrocarbons at temperatures from 773 to 873 K among all the catalysts tested so far.[17,18] On the other hand, Co catalysts also decomposed hydrocarbons or CO to form nanoscale carbon materials, while their catalytic activity and life were inferior to those of supported Ni catalysts.[19−21] However, supported Co catalysts can form SWCNT and MWCNT with relatively high selectivity, compared to supported Ni. For the preparation of SWCNT and MWCNT, CO, benzene, or acetylene is frequently utilized.[19−21] These substrates diluted with hydrogen are contacted with Co catalysts at a temperature range of 873 to 1273 K to form SWCNT and MWCNT. Hydrogen cofed can eliminate amorphous carbons deposited on SWCNT and MWCNT during the reactions, for the pyrolytic decomposition of benzene or acetylene in addition to the catalytic decomposition taking place inevitably at higher reaction temperatures.[19,22] In contrast, methane is not decomposed pyrolytically but catalytically at a temperature range from 873 to 1273 K, because it is the most kinetically stable hydrocarbon. Therefore, methane is one of the most ideal carbon sources for the synthesis of SWCNT and MWCNT. When MWCNT and SWCNT are produced from methane, we can easily neglect the contribution of carbons formed by its pyrolytic decomposition; i.e., only the morphology of carbons formed by the catalytic

* Author to whom correspondence should be addressed. E-mail: stakenak@o.cc.titech.ac.jp. Tel.: 81-3-5734-2626. Fax: 81-3-5734-2879.
† Tokyo Institute of Technology.
‡ Western Hiroshima Prefecture Industrial Institute.

10.1021/jp048827t CCC: $27.50
Published on Web 07/10/2004

decomposition would be investigated. Methane decomposition over Co catalysts has been examined by some research groups.[23−26] However, available literature on the synthesis of nanoscale carbons from methane is significantly smaller at the present stage compared to that from CO, benzene, and acetylene. In particular, there are few studies on the structure of carbons formed under different conditions or on the structural change of Co species during the reaction. In addition, there is a lack of consensus for the growth mechanism of nanoscale carbons over Co catalysts. To make clear the growth mechanism of nanoscale carbons through methane decomposition over supported Co catalysts, the states of Co species and the structures of carbons should be investigated in detail.

In this study, methane decomposition was performed over Co catalysts supported on different supports to make clear the factors which determine their catalytic activity and life for the reactions. The growth mechanisms of carbon nanofibers and carbon nanotubes by Co catalysts will be discussed on the basis of the structure of carbons thus formed as well as the structural change of Co species in the catalysts during the methane decomposition.

2. Experimental Section

Supported Co catalysts used in this study were prepared by a conventional impregnation method. MgO (JRC-MGO1, specific surface area = 55 $m^2\ g^{-1}$), Al_2O_3 (JRC-ALO4, specific surface area = 177 $m^2\ g^{-1}$), SiO_2 (Cab-O-Sil supplied from Cabot Co., specific surface area = 200 $m^2\ g^{-1}$), and TiO_2 (JRC-TIO4, specific surface area = 50 $m^2\ g^{-1}$) were utilized as catalytic supports. JRC-MGO1, JRC-ALO4, and JRC-TIO4 were supplied from the Catalytic Society of Japan as reference catalysts. The catalytic supports were impregnated with an aqueous solution of $Co(NO_3)_2 \cdot 6H_2O$ at 363 K. The solvent was evaporated to dryness at 363 K. The dried samples were calcined at 873 K for 5 h under air.

Methane decomposition was carried out in a conventional gas flow system with fixed catalyst bed. The catalyst samples (0.060 g) were packed in a tube made from quartz (inner diameter = 20 mm and length = 800 mm). Prior to the methane decomposition, the catalysts were treated with hydrogen at 773 K for 1 h. Then, hydrogen remaining in the reactor was purged out with Ar at the reaction temperatures of methane decomposition. Methane decomposition was initiated by contact of the reduced catalysts with methane (101 kPa and 50 mL min^{-1}). During the reaction, a portion of the effluent gases from the catalyst bed was sampled out and analyzed by GC. Conversion of methane during the methane decomposition was estimated from the concentration of hydrogen and methane in the effluent gases from the catalyst bed, assuming that the reaction, $CH_4 \rightarrow C + 2H_2$, proceeded selectively. In fact, the formation of hydrogen was observed as a gaseous product in addition to a trace of CO during the methane decomposition.

X-ray absorption spectra (XANES and EXAFS) were measured on the beam line BL-9A at Photon Factory in the Institute of Materials Structure Science for High Energy Accelerator Research Organization at Tsukuba in Japan (Proposal No.: 2002G255). Co K-edge XANES and EXAFS of supported Co catalysts were measured with a fluorescence mode with a Si(111) two-crystal monochlomator at room temperature. The spectrum of Co foil was measured in the transmission mode at room temperature. To prepare the catalyst samples after the methane decomposition for the measurements of XANES and EXAFS, the catalyst samples which had been reduced with hydrogen at 773 K were contacted with methane at the required temperatures. After the reaction, the catalyst samples were cooled to room temperature under an Ar stream and they were packed in a bag made from polyethylene under argon atmosphere. The analysis of EXAFS data was performed by using an EXAFS analysis program, REX (Rigaku Co.). For EXAFS analysis, the oscillation was extracted from the EXAFS data by a spline smoothing method. The oscillation was normalized by the edge height around 70−100 eV above the threshold. The Fourier transformation of k^3-weighted EXAFS oscillation was performed over a k-range of 3.5−14.0 $Å^{-1}$. Inversely Fourier transformed data for each Fourier peak were analyzed by a curve-fitting method, using theoretical phase shifts and amplitude functions derived by the FEFF8 program.[27]

SEM and TEM images of carbons deposited on the catalysts by methane decomposition were measured using a Hitachi FE-SEM S-800 (field emission gun scanning electron microscope) and a JEOL JEM-3000F, respectively.

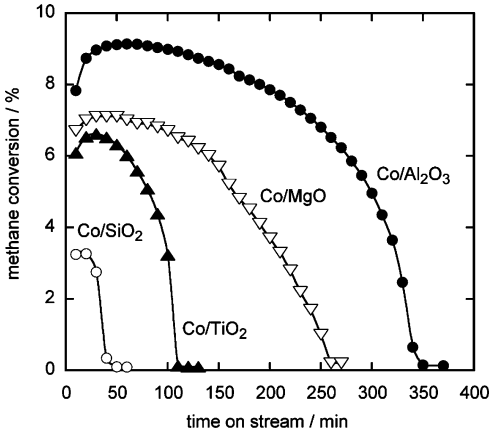

Figure 1. Change of the methane conversion as a function of time on a stream of methane in methane decomposition at 773 K over Co catalysts supported on different supports. Catalysts = 0.060 g, loading of Co = 20 wt %, $P(CH_4)$ = 101 kPa, and flow rate = 50 mL min^{-1}.

3. Results and Discussion

3.1. Methane Decomposition over Co Catalysts Supported on Different Supports. Figure 1 shows change of the methane conversion as a function of time on a stream of methane during methane decomposition at 773 K over Co catalysts supported on different supports. Methane decomposition proceeded over all the catalysts irrespective of the types of supports to form hydrogen selectively in addition to a trace of CO as gaseous product. Methane conversion at the early period of the reaction (<30 min) strongly depended on the types of catalytic supports. The catalytic activity at the early period became higher in the order of $Co/Al_2O_3 > Co/MgO > Co/TiO_2 > Co/SiO_2$. Methane conversion for all the catalysts declined gradually or quickly with time on stream, and finally all the catalysts lost activity completely for the methane decomposition. The catalytic life was also dependent on the types of catalytic supports; i.e., the life was longer in the order of $Co/Al_2O_3 > Co/MgO > Co/TiO_2 > Co/SiO_2$. The carbon yields until the complete deactivation of these catalysts were evaluated by integrating the formation rate of hydrogen against time on stream, assuming that methane decomposition, $CH_4 \rightarrow C + 2H_2$, proceeded selectively. The carbon yield, C/Co, which was moles of carbons deposited on 1 mol of Co in the catalysts, was estimated to be 277 for Co/Al_2O_3, 139 for Co/MgO, 73 for Co/TiO_2, and 12 for Co/SiO_2.

Figure 2 shows XRD patterns of supported Co catalysts after the reduction with hydrogen at 773 K and of catalytic supports.

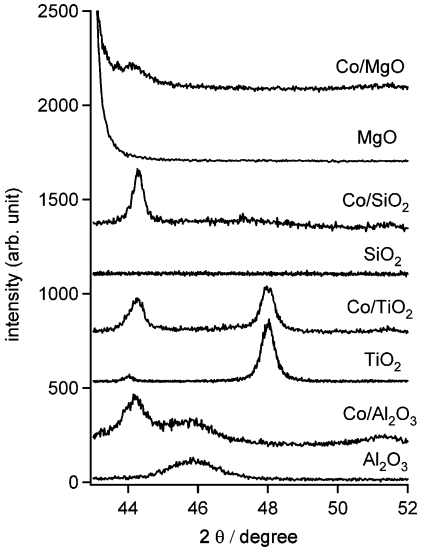

Figure 2. XRD patterns of supported Co catalysts and of catalytic supports. Loading of Co = 20 wt %.

For all the XRD patterns of the supported Co catalysts, a diffraction line due to Co metal was observed at ca. 44 deg. Because the diffraction line due to Co metal was overlapped with that due to MgO, Al_2O_3, or TiO_2, an average crystallite size of Co metal could not be estimated from the full width at half-maximum of the peak. Nevertheless, it should be noted that the widths of a peak due to Co metal for Co/Al_2O_3 and Co/MgO were greater than those for Co/SiO_2. Thus, it is likely that an average crystallite size of Co metal on Co/Al_2O_3 and Co/MgO was smaller than that on Co/SiO_2. As described above, the catalytic performance (the activity, life, and carbon yield) of Co/Al_2O_3 and Co/MgO for the methane decomposition was superior to that of Co/SiO_2. These results implied that Co metals with smaller crystallite sizes showed higher activity and longer life for the methane decomposition at 773 K.

Figure 3 shows SEM images of carbons deposited on the supported Co catalysts by methane decomposition at 773 K. SEM images of carbons were measured after the complete deactivation of the catalysts. It was found that carbons deposited on all the catalysts grew with a filamentous structure. The diameter ranges of carbon nanofibers observed in the SEM images seem to be relatively uniform for the four catalysts; i.e., their diameters ranged from 10 to 30 nm. As described below, Co metal particles were present at the tip of carbon nanofibers formed at 773 K. The diameter of Co metal particles present at the tip of carbon nanofibers was similar to that of the corresponding fiber. The diameter range of carbon nanofibers observed in the SEM images was almost the same (10−30 nm) for the four catalysts, although XRD studies implied that average crystallite sizes of Co metal were changed by the types of catalytic supports. It is likely that Co metal particles with diameters from 10 to 30 nm grew carbon nanofibers preferentially through the methane decomposition at 773 K, while ones larger than 30 nm or smaller than 10 nm were inactive for the formation of carbon nanofibers.

Figure 4 shows TEM images of carbons deposited on Co/Al_2O_3 (images a and b) and on Co/SiO_2 (images c and d) by methane decomposition at 773 K. Co metal particles were observed at the tip of carbon nanofibers for both the catalysts (images a and c). The diameter of carbon nanofibers was almost the same as that of Co metal particles present at the tip of the fibers. The exposed surface of Co metal particles at the tip of the fibers decomposed methane into carbon and hydrogen.[20,28,29]

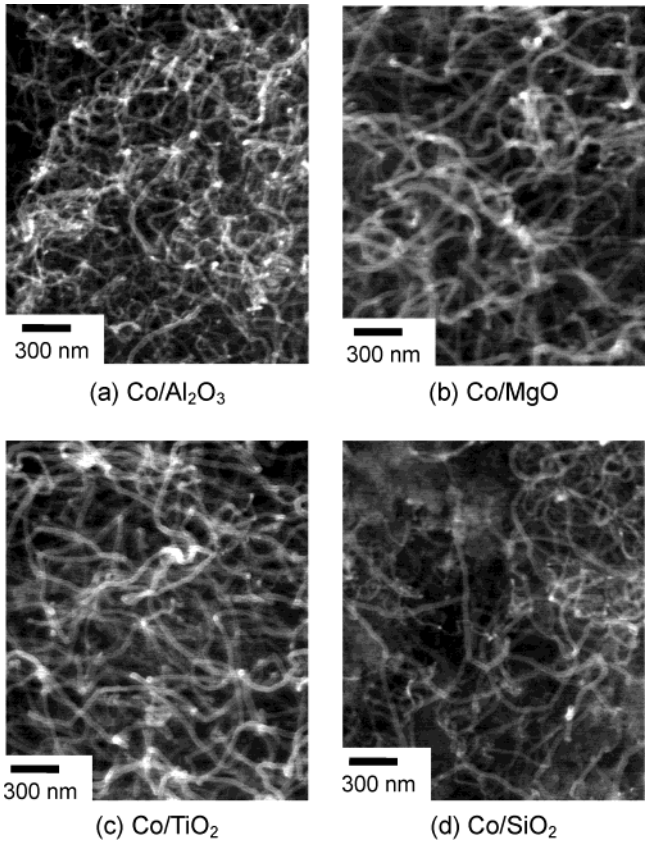

Figure 3. SEM images of carbon nanofibers deposited on supported Co catalysts by methane decomposition at 773 K. Loading of Co = 20 wt %.

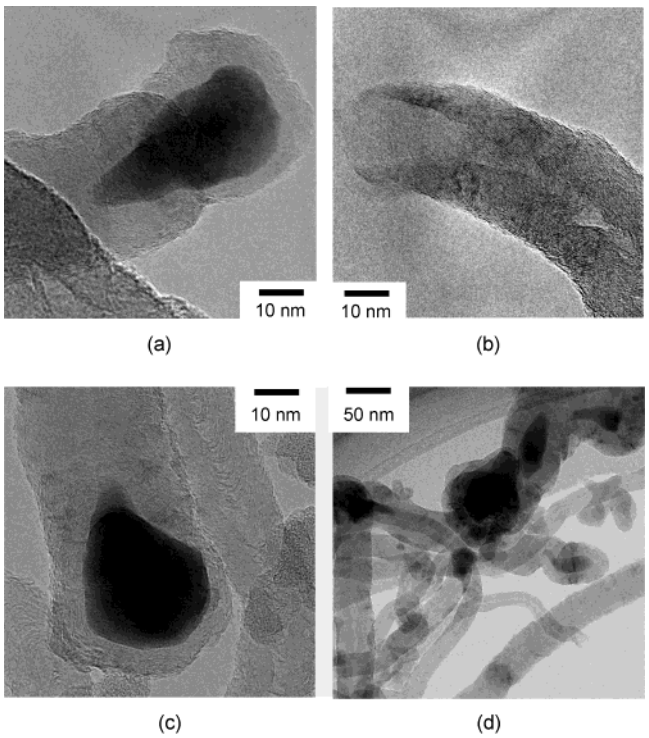

Figure 4. TEM images of carbons deposited on Co/Al_2O_3 (images a and b) and on Co/SiO_2 (images c and d) by the methane decomposition at 773 K. Loading of Co = 5 wt %.

Carbon atoms deposited on the Co metal surface were diffused in the interior and/or on the surface of the metal, and they were precipitated from the other surface of the metal to grow carbon nanofibers. The graphite layers of carbon nanofibers formed

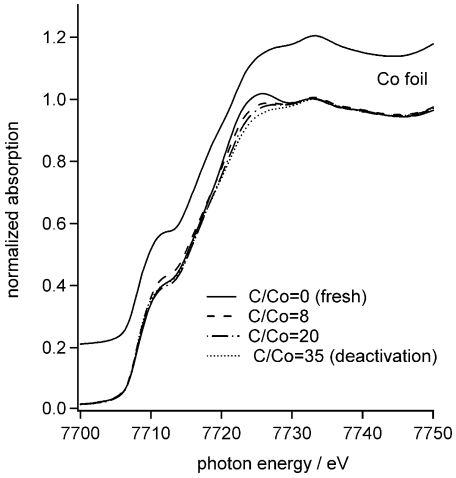

Figure 5. Co K-edge XANES spectra of Co/SiO_2 catalysts before and after methane decomposition at 773 K and of Co foil. Loading of Co = 5 wt %.

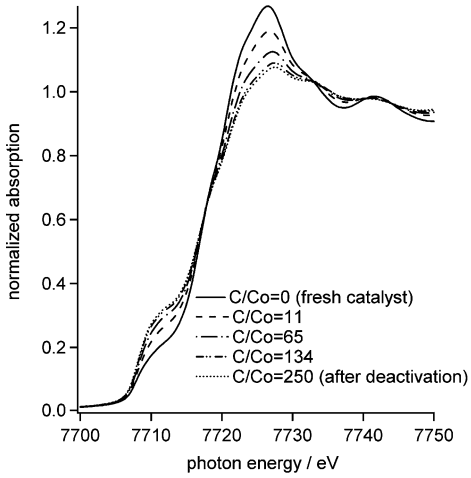

Figure 6. Co K-edge XANES spectra of Co/Al_2O_3 catalysts before and after methane decomposition at 773 K. Loading of Co = 5 wt %.

on Co/Al_2O_3 and Co/SiO_2 were canted slightly against the fiber axis, i.e., fish-bone typed carbon nanofibers, as observed in the images b and c.[24] Similar carbon nanofibers were formed by the methane decomposition over Co/TiO_2 and Co/MgO at 773 K, although their TEM images were not shown. Thus, methane decomposition over supported Co catalysts at 773 K produced fish-bone-typed carbon nanofibers mainly, irrespective of the types of catalytic supports.

As for the Co/SiO_2 catalyst, Co metal particles of sizes larger than 30 nm were also frequently observed in addition to those with sizes of 10−30 nm, as shown in TEM image d. In contrast, Co metal particles larger than 30 nm were rarely observed in TEM images for Co/Al_2O_3 or Co/MgO after the methane decomposition at 773 K. It should be noted that Co metal particles of sizes larger than 30 nm did not form long carbon nanofibers, while ones of 10−30 nm formed them preferentially. Co metal particles of sizes larger than 30 nm were mostly present in short carbon nanofibers or they were covered with thick layers of carbons of the spherical shape. These results suggested that Co metal particles of sizes larger than 30 nm were inactive for the formation of long carbon nanofibers. As described earlier, the catalytic life and carbon yield of Co/Al_2O_3 and Co/MgO for the methane decomposition at 773 K were significantly superior to those for Co/SiO_2. Catalytic performance of Co/SiO_2 for methane decomposition would be poor, because the fraction of Co metal particles larger than 30 nm in all the metal particles on Co/SiO_2 was higher compared to those for Co/Al_2O_3 and Co/MgO. It is worth while noting that all the Co metal particles observed in the TEM images were wrapped with thick layers of deposited carbons irrespective of their sizes. TEM images shown in Figure 4 were measured after the complete deactivation of the catalysts for the methane decomposition at 773 K. Thus, it is likely that supported Co catalysts were deactivated by the coverage of Co metal particles with graphite layers.[30,31]

Figure 5 shows Co K-edge XANES spectra of Co/SiO_2 catalysts before and after methane decomposition at 773 K and of Co foil. Methane decomposition was terminated compulsorily at a certain amount of carbons deposited (C/Co = 8, 20, and 35). Carbon yield C/Co at the complete deactivation of Co/SiO_2 was estimated to be 35. XANES spectrum of the fresh Co/SiO_2 catalyst was similar to that of Co foil, although the absorption at 7722 eV for the catalyst was slightly stronger than that for Co foil. Therefore, most Co species in the fresh Co/SiO_2 were present as Co metal. Contact of methane with the catalyst decreased slightly the absorption at 7722 eV in the XANES spectra. In general, the absorption at around 7722 eV in Co K-edge XANES spectra becomes stronger when Co species are oxidized.[32,33] These results indicate that Co species on Co/SiO_2 were not reduced completely prior to the methane decomposition, although most Co species were present as Co metal. The oxidized Co species would be reduced gradually into Co metal during the methane decomposition. Co metal particles on the fresh Co/SiO_2 were present on SiO_2, while they interacted with carbons directly after the methane decomposition, as shown in TEM images of Figure 4. Co species in Co metal which were interacted directly with SiO_2 in the fresh Co/SiO_2 (interfacial $Co-SiO_2$ sites) may be partially oxidized through Si−O−Co bonds. The Si−O−Co bonds should be lost due to the carbon deposition on Co metal particles during the methane decomposition. The XANES spectrum of the deactivated Co/SiO_2 catalyst was well consistent with that of Co foil, suggesting that Co species in the deactivated catalyst were present as Co metal. We have reported that Ni species changed from Ni metal to Ni carbide species at the deactivation stage of Ni/SiO_2 for the methane decomposition, while they were present as Ni metal when the catalyst decomposed methane actively.[34]

Figure 6 shows Co K-edge XANES spectra of Co/Al_2O_3 catalysts before and after methane decomposition at 773 K. The amount of carbons deposited on Co/Al_2O_3 was changed from 11 to 250, where the catalyst was deactivated completely. For the XANES spectrum of the fresh Co/Al_2O_3, absorption at around 7712 eV, which is characteristic of Co metal, was observed. In addition, the XANES spectrum of the fresh Co/Al_2O_3 showed a stronger absorption at around 7725 eV compared to that of the fresh Co/SiO_2 (Figure 5). Thus, the fraction of the oxidized Co species in all the Co species on the fresh Co/Al_2O_3 was higher than that for the fresh Co/SiO_2. No diffraction lines due to the compounds containing Co species except for Co metal were observed in the XRD pattern of the fresh Co/Al_2O_3 catalyst, although the spectrum was not shown. On the basis of these results, Co species in the fresh Co/Al_2O_3 were present as dispersed Co oxide species in addition to Co metal. It was reported that Co species in Co/Al_2O_3 were stabilized as highly dispersed Co oxides.[35,36] The dispersed Co oxide species on Al_2O_3 were not reduced easily with hydrogen at temperatures <773 K, while crystallized CoO and Co_3O_4 on Al_2O_3 could be reduced with hydrogen under the corresponding conditions.[35,36] However, contact of methane with Co/Al_2O_3 catalysts decreased the absorption at 7725 eV and increased the absorption at 7712 eV. Therefore, the oxidized Co species

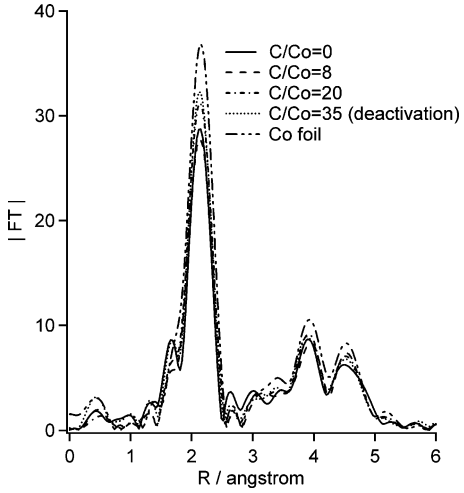

Figure 7. Fourier transforms of Co K-edge k^3-weighted EXAFS for Co/SiO_2 catalysts before and after methane decomposition at 773 K and of Co foil. Loading of Co = 5 wt %.

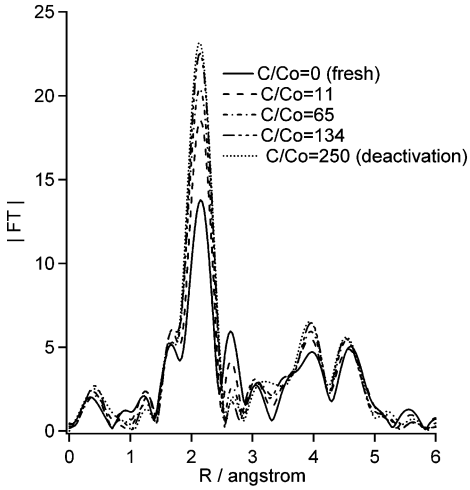

Figure 8. Fourier transforms of Co K-edge k^3-weighted EXAFS for Co/Al_2O_3 catalysts before and after methane decomposition at 773 K. Loading of Co = 5 wt %.

TABLE 1: Curve-Fitting Results for Co K-Edge EXAFS of Co/SiO_2 and Co/Al_2O_3

catalysts	C/Co	CN[a]	R/Å[b]	σ/Å[c]
Co/SiO_2	0 (fresh)	6.9 (±0.9)	2.49	0.064
	8	8.3 (±1.0)	2.49	0.071
	20	8.9 (±1.0)	2.49	0.070
	35 (deactivatn)	8.6 (±1.0)	2.49	0.078
Co/Al_2O_3	0 (fresh)	4.4 (±0.5)	2.48	0.071
	11	5.5 (±0.7)	2.49	0.072
	65	6.3 (±0.9)	2.48	0.073
	134	6.7 (±0.8)	2.48	0.071
	250 (deactivatn)	6.9 (±0.9)	2.48	0.071

[a] Coordination number of Co−Co. [b] Interatomic distance of Co−Co. [c] Debye−Waller factor.

in the fresh Co/Al_2O_3 catalyst were reduced with methane gradually into Co metal during the reaction. The absorption at 7725 eV for XANES spectrum of the deactivated Co/Al_2O_3 was slightly stronger than those for Co foil (Figure 5). Thus, a part of Co species in Co/Al_2O_3 catalyst was present as Co oxides after the complete deactivation for the methane decomposition at 773 K.

Figure 7 shows Fourier transforms of Co K-edge k^3-weighted EXAFS (RSFs: radial structural functions) for Co/SiO_2 before and after methane decomposition at 773 K and for Co foil. The RSF of the fresh Co/SiO_2 was well consistent with that of Co foil, although the intensity of each peak for the catalyst was smaller than that of Co foil. This result indicated that most of Co species in the fresh Co/SiO_2 were present as Co metal. Contact of methane with Co/SiO_2 brought about a slight increase in the intensity of the peak at 2.1 Å, which was assigned to Co−Co bonds in Co metal. The increase in the peak intensity at 2.1 Å would result from an increase of an average crystallite size of Co metal during the methane decomposition over Co/SiO_2 catalyst at 773 K. Curve-fitting analysis for Co K-edge EXAFS of Co/SiO_2 also suggested the structural change of Co metal during the methane decomposition. Table 1 shows the results of curve-fitting for the peak at around 2.1 Å in the RSF of Co/SiO_2. For the curve-fitting of Co K-edge EXAFS, inversely Fourier transformed data for the Fourier peak in a R-range of 1.4−2.4 Å were analyzed. The peak at 2.1 Å for all the RSFs of Co/SiO_2 could be assigned to a specific Co−Co bond in Co metal by the curve-fitting. The coordination number of Co−Co bonds in the fresh Co/SiO_2 was estimated to be 6.9. Carbon deposition of C/Co = 8 on Co/SiO_2 increased the coordination number of Co−Co bonds from 6.9 to 8.3 without changing their interatomic distance. However, further deposition of carbons to C/Co = 20 and 35 did not change appreciably the coordination number or the interatomic distance of Co−Co bonds. These results suggested that Co metal crystallites on the fresh Co/SiO_2 were aggregated into larger ones at early period of methane decomposition. As described earlier, Co metal particles with sizes from 10 to 30 nm formed carbon nanofibers preferentially by the methane decomposition at 773 K, while ones larger than 30 nm were inactive for their growth. It is likely that Co/SiO_2 was deactivated quickly for the methane decomposition as shown in Figure 1, because Co metal particles in the catalyst were aggregated at very early period of the reaction to form ones larger than 30 nm.

Similar aggregation of Co metal crystallites during the methane decomposition could be confirmed for Co/Al_2O_3 catalyst from Co K-edge EXAFS. Figure 8 shows Fourier transforms of Co K-edge k^3-weighted EXAFS (RSFs) for Co/Al_2O_3 before and after the methane decomposition at 773 K. As for all the RSFs of Co/Al_2O_3, the strongest peak was observed at 2.1 Å, where the RSF of Co foil also showed the peak due to Co−Co bonds. The peak at 2.1 Å for the fresh Co/Al_2O_3 catalyst was significantly smaller than that for the fresh Co/SiO_2 (Figure 7). This result implies that an average crystallite size of Co metal on the fresh Co/Al_2O_3 was smaller compared to that on the fresh Co/SiO_2. The peak at 2.1 Å due to Co−Co bonds in Co metal for the RSFs of Co/Al_2O_3 became gradually stronger as the amount of carbons deposited from methane increased. In addition, a peak was observed at around 2.7 Å in the RSF of the fresh Co/Al_2O_3 and the peak became smaller with the larger amount of carbons deposited on the catalysts. XANES spectra and XRD pattern of the Co/Al_2O_3 suggested the formation of dispersed Co oxide species in addition to Co metal. Therefore, the peak at 2.7 Å would be deduced to Co−Co bonds in the dispersed Co oxides. On the basis of these results, dispersed Co oxides in Co/Al_2O_3 catalyst were reduced with methane into Co metal during the methane decomposition.

Curve-fitting results for Co K-edge EXAFS of Co/Al_2O_3 were shown in Table 1. The peak at around 2.1 Å for all the Co/Al_2O_3 could be assigned to a specific Co−Co bond in Co metal. The coordination number of Co−Co bonds for the fresh Co/Al_2O_3 was estimated to be 4.4, which was significantly smaller than that for the fresh Co/SiO_2. The coordination number of

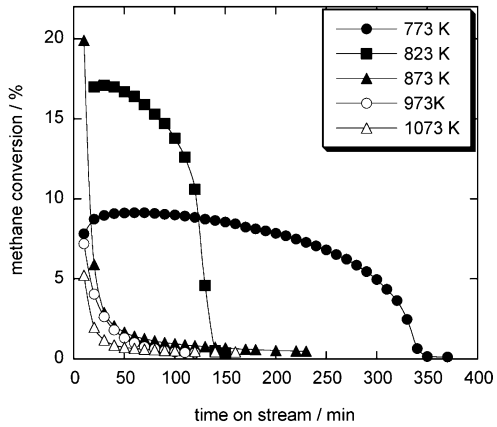

Figure 9. Change of the methane conversion with time on stream in the methane decomposition over Co/Al_2O_3 catalysts at different temperatures. Catalysts = 0.060 g, loading of Co = 20 wt %, $P(CH_4)$ = 101 kPa, and flow rate = 50 mL min^{-1}.

Co−Co bonds for the fresh Co/Al_2O_3 increased gradually as the amount of carbons deposited on the catalyst increased. The coordination number of Co−Co bonds was changed to 6.9 after the complete deactivation of Co/Al_2O_3. The increase of the coordination numbers of a specific Co−Co bond in Co metal on Co/Al_2O_3 catalyst during the methane decomposition would result from the reduction of Co oxides with methane into Co metal and/or from the aggregation of Co metal crystallites. It is worth while noting that the coordination number of Co−Co bonds for Co/Al_2O_3 during the methane decomposition (ca. 6−7) was significantly smaller than that for Co/SiO_2 (ca. 8−9). Thus, an average crystallite size of Co metal on the Co/Al_2O_3 during the reaction should be smaller than that for the Co/SiO_2, although Co metal crystallites were aggregated during the reaction for both the catalysts. As described earlier, Co/Al_2O_3 was a more effective catalyst for the methane decomposition than Co/SiO_2 from a viewpoint of the catalytic life and carbon yield. It is likely that Co/Al_2O_3 catalyst showed longer catalytic life and higher carbon yield for methane decomposition because Co metal particles on the catalyst were not aggregated into too large particles (>30 nm) during the reaction. This would be attributed to the strong interaction of Co species and Al_2O_3 support.[35,36] A similar conclusion was proposed in the case of the synthesis of carbon nanotubes by the decomposition of CO and acetylene over Co/MgO catalysts.[11,26,37] When the Co species was supported on a MgO support, Co−Mg−O solid solutions were formed. The solid solutions did not produce larger Co metal particles by the reduction with hydrogen prior to the reaction but produced fine particles during the synthesis of carbon nanotubes. The fine Co metal particles produced carbon nanotubes selectively. In our case, the oxidized Co species in Co/Al_2O_3 catalyst were reduced with methane gradually during the methane decomposition to form Co metal particles active for the growth of carbon nanofibers and carbon nanotubes.

3.2. Catalytic Performance of Co/Al_2O_3 Catalysts. As described earlier, Co/Al_2O_3 catalyst showed the highest activity and the longest life for methane decomposition at 773 K among all the supported Co catalysts tested in the present study. Co/Al_2O_3 produced fish-bone typed carbon nanofibers by the methane decomposition at 773 K as shown in Figure 4. The structure of carbons produced by the reaction would depend on the temperatures of methane decomposition. Thus, the effects of the reaction temperatures on the catalytic performance of Co/Al_2O_3, the structure of Co metal, and the shape of carbons formed from methane were investigated. Figure 9 shows change of the methane conversion with time on stream in the methane decomposition over Co/Al_2O_3 catalysts at different temperatures. Reaction temperatures were changed from 773 to 1073 K. Methane conversion at a very early period of the reaction increased when the reaction temperatures were raised from 773 to 873 K. However, reaction temperatures higher than 873 K resulted in a decrease in the methane conversion at an early period of the reaction. Catalytic life of Co/Al_2O_3 for the reaction became shorter with higher reaction temperatures. Thus, the carbon yield, C/Co, until the complete deactivation of the catalyst was lower with higher reaction temperatures; i.e., C/Co = 277 for 773 K, 227 for 823 K, 66 for 873 K, 28 for 973 K, and 22 for 1073 K.

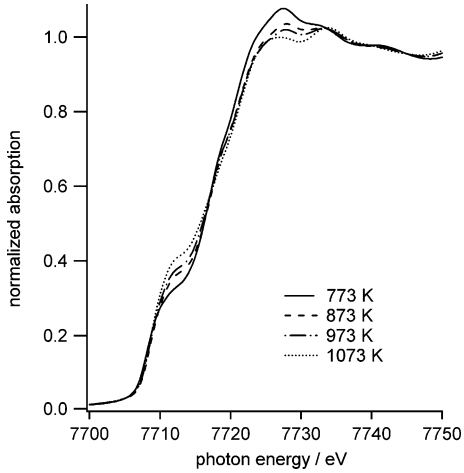

Figure 10. Co K-edge XANES spectra of Co/Al_2O_3 catalysts deactivated by the methane decomposition at different temperatures. Loading of Co = 5 wt %.

Figure 10 shows Co K-edge XANES spectra of Co/Al_2O_3 catalysts deactivated for the methane decomposition at different temperatures. Absorption at around 7712 eV in XANES spectra of Co/Al_2O_3 became stronger, and that at 7725 eV became smaller with higher reaction temperatures. The former and latter peaks were characteristic of Co metal and Co oxides, respectively, as described in the preceding section. On the basis of these XANES spectra, the fraction of oxidized Co species in the catalyst became lower with a rise of the reaction temperatures. Most Co species in the catalysts deactivated at temperatures ≥873 K would be present as Co metal, because their XANES spectra were similar to that of Co foil.

Fourier transforms for Co K-edge EXAFS of Co/Al_2O_3 (RSFs) also suggested the structural change of Co species depending on the reaction temperatures. The results are shown in Figure 11. The RSFs for all the catalysts were well consistent with that of Co foil in Figure 7 irrespective of different reaction temperatures, suggesting that most Co species in the deactivated catalysts were present as Co metal. A peak was observed at 2.1 Å for all the RSFs of Co/Al_2O_3, and the intensity became higher with a rise of reaction temperatures. The results of curve-fitting for the peak around 2.1 Å are listed in Table 2. The peak was assigned to a type of Co−Co bonds in Co metal for all the EXAFS spectra of Co/Al_2O_3. The coordination number of a specific Co−Co bond in Co metal increased gradually with higher reaction temperatures. These results implied that the aggregation of Co metal crystallites on Co/Al_2O_3 was enhanced when the reaction temperatures became higher. Nevertheless, it should be noted that the coordination number (CN) of Co−Co bonds for the Co/Al_2O_3 catalyst deactivated at 1073 K (CN = 8.0) was smaller than that for the Co/SiO_2 catalyst deactivated at 773 K (CN = 8.6). This result implies that Co/Al_2O_3 formed smaller Co metal crystallites during the methane decomposition

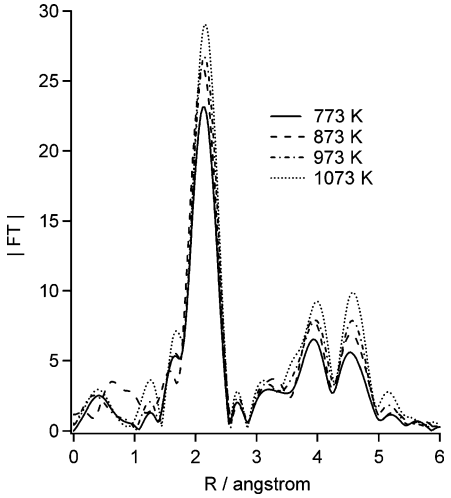

Figure 11. Fourier transforms of Co K-edge k^3-weighted EXAFS spectra for Co/Al_2O_3 catalysts deactivated by the methane decomposition at different temperatures. Loading of Co = 5 wt %.

TABLE 2: Curve-Fitting Results for Co K-Edge EXAFS of Co/Al_2O_3 Deactivated for Methane Decomposition at Different Temperatures

temp/K	CN[a]	R/Å[b]	σ/Å[c]
773	6.9 (±0.9)	2.48	0.071
873	7.4 (±0.7)	2.49	0.068
973	7.8 (±0.8)	2.48	0.070
1073	8.0 (±0.9)	2.48	0.069

[a] Coordination number of Co−Co bonds. [b] Interatomic distance of Co−Co bonds. [c] Debye−Waller factor.

compared to Co/SiO_2, due to the stronger interaction between Co and Al_2O_3.[35,36]

Figures 12−14 show TEM images of carbons formed by the methane decomposition over Co/Al_2O_3 catalysts at 873, 973, and 1073 K, respectively. TEM images of carbons formed at 773 K were shown in Figure 4. These TEM images were measured after the complete deactivation of the catalysts. Methane decomposition at 873 K produced MWCNT preferentially as shown in Figure 12. Outer and inner diameter ranges of MWCNT were 15−30 and 5−15 nm, respectively. The graphite layers of MWCNT were parallel to the axis of the tubes (image d). In addition, several knots were often observed in the MWCNT, i.e., bamboolike MWCNT. It is worth while noting that most Co metal particles observed in TEM images of the catalyst deactivated at 873 K were present at the tip of MWCNT, as can be confirmed in the images b and c. Taking into consideration the growth mechanism of MWCNT proposed by many research groups,[20,28,29,38] it is reasonable to suppose that Co metal particles at the tip of MWCNT decomposed methane to elongate the lengths of tubes, i.e., the tip growth mechanism. As shown in TEM images of Figure 4, Co metal particles were present at the tip of carbon nanofibers, when the methane decomposition was performed over Co/Al_2O_3 at 773 K. From these results described above, we concluded that carbon nanotubes and carbon nanofibers were formed by the tip growth mechanism through the methane decomposition at temperatures ≤873 K; i.e., Co metal particles present at the tip of carbon nanotubes and nanofibers decomposed methane into carbon and hydrogen atoms and the carbon atoms were diffused in the interior and/or on the surface of the metal to form the tubes and fibers.

Methane decomposition over Co/Al_2O_3 at 973 K also formed MWCNT mainly, as shown in Figure 13 (images a and c). The

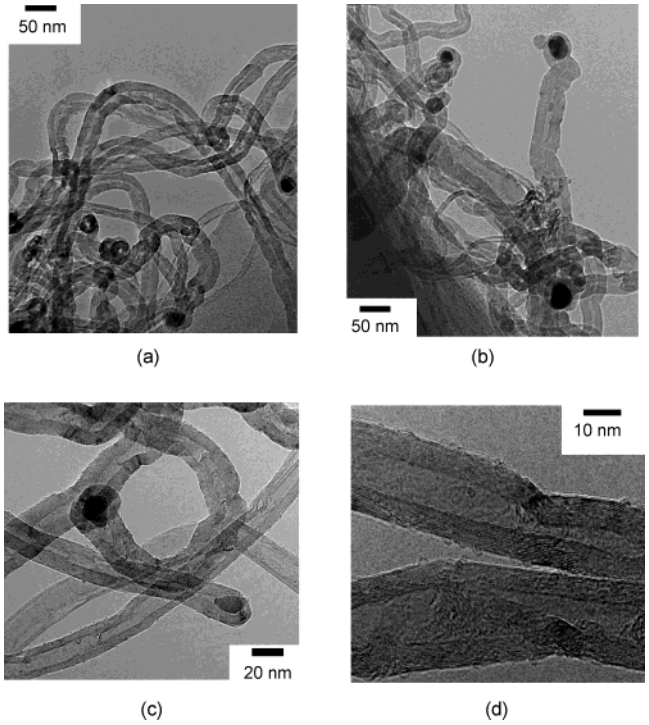

Figure 12. TEM images of carbons deposited on Co/Al_2O_3 by methane decomposition at 873 K. Loading of Co = 5 wt %.

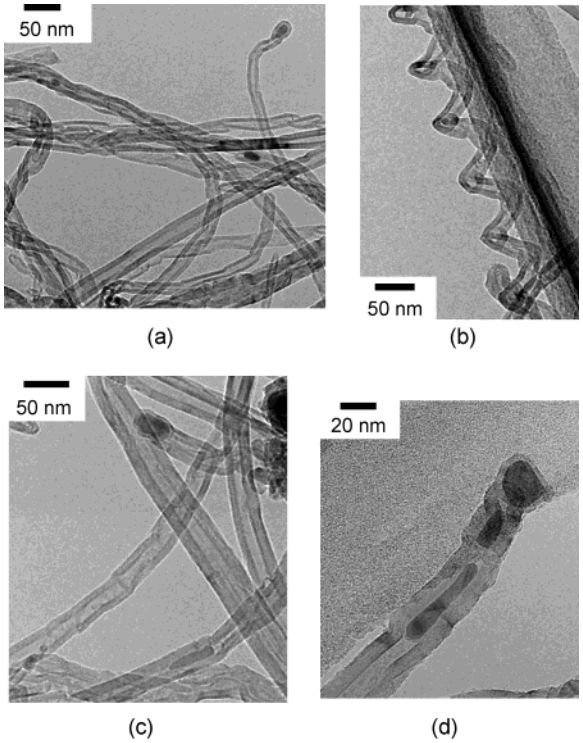

Figure 13. TEM images of carbons deposited on Co/Al_2O_3 by methane decomposition at 973 K. Loading of Co = 5 wt %.

shape of MWCNT formed at 973 K was relatively straight, whereas most tubes formed at 873 K were roundish (Figure 12). In addition, the wall of MWCNT formed at 973 K was slightly thinner than that formed at 873 K, while their outer diameters were similar to each other. Except for MWCNT, helically coiled carbon nanotubes (image b) and bamboolike carbon nanotubes (images c and d) were formed at 973 K. On the TEM images of carbons formed at 973 K, Co metal particles were frequently observed in the hollow of MWCNT (images c

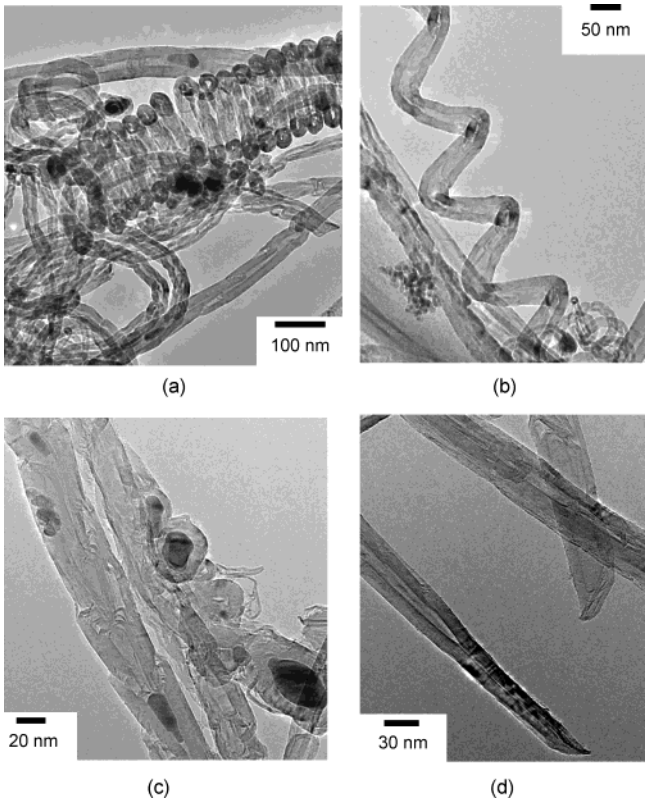

Figure 14. TEM images of carbons deposited on Co/Al_2O_3 by methane decomposition at 1073 K. Loading of Co = 5 wt %.

and d) as well as the tip of them (images a and d). The shapes of Co metal particles were different depending on their positions observed in the TEM images. For example, Co metal particles present in the hollow of MWCNT were elongated to the direction of the axis of MWCNT, while the shapes of ones present at the tip of MWCNT seemed to be of circle or ellipse in the TEM images. On the basis of these TEM images, it is difficult to suppose that Co metal particles of the solid state catalyzed the methane decomposition to grow carbon nanotubes. It is likely that Co metal particles on Co/Al_2O_3 were present in the state with high fluidity, i.e., the liquid state during the methane decomposition at 973 K. The melting point of Co metal is remarkably higher than 973 K. However, the melting point of Co metal decreased as the crystallite sizes of the metal became smaller.[39,40] In addition, carbon atoms from methane were dissolved in the interior of Co metal particles to form carbon naotubes, which would decrease melting points of the metal.[39−41]

When the reaction temperature of methane decomposition increased to 1073 K, the shapes of the carbons formed were furthermore changed (Figure 14). As shown in image a, the content of straight MWCNT in all the carbons formed at 1073 K was significantly low. Instead of the straight MWCNT, the formations of helically coiled carbon nanotubes (images a and b) and of bamboolike carbon nanotubes (images c and d) were enhanced in the reaction at 1073 K. Co metal particles were often present in the hollow of bamboolike carbon nanotubes (image c), but they were seldom observed at the tip of the carbon nanotubes. In addition, the number of Co metal particles observed in the TEM images of the carbons formed at 1073 K was significantly smaller than those of the carbons formed at 873 K (Figure 12) and 973 K (Figure 13). As for bamboolike carbon nanotubes and MWCNT formed at 1073 K, closed tips were often observed (image d). In contrast, Co metal particles were always present at the tip of carbon nanotubes and nanofibers when the methane decomposition was performed at temperatures ≤873 K. These results strongly suggest that the growth mechanism of carbon nanotubes and nanofibers through the methane decomposition over the supported Co catalysts depends on the reaction temperatures. Carbon nanatubes and carbon nanofibers were formed through the tip growth model at temperatures ≤873 K. As for the methane decomposition at temperatures ≥973 K, some carbons may be formed by the tip growth mechanism. Co metal particles would be present at the tip of carbon nanotubes intrinsically at an early period of the reaction; however, Co metal particles may be divided into smaller ones during the reaction and their smaller ones were left in the hollow of the tubes, because of high fluidity of the metal at temperatures ≥973 K. Except for the tip growth model, the base growth mechanism cannot be neglected for the growth of carbon nanotubes during the methane decomposition at 1073 K, because Co metal particles were not observed anywhere in many carbons and closed tips of carbon nanotubes were frequently observed. In the case of the synthesis of SWCNT and MWCNT through the decomposition of hydrocarbons over supported Co catalysts, the base growth mechanism was often proposed.[42−44] For the base growth mechanism of carbon nanotubes, Co metals are always present on the catalytic supports during the growth of the carbons. The formation of carbon nanotubes by the base growth mechanism would be enhanced as the interaction of the catalytic supports with Co metal particles becomes stronger. It is likely that the interaction of Co metal with Al_2O_3 became stronger due to the formation of their compound oxides around Co metal particles at higher temperatures. The strong interaction between Co metal and Al_2O_3 at higher temperatures would prevent the detachment of Co metal from Al_2O_3 support during the reaction.

4. Conclusion

We concluded as follows on the basis of the results described above: (1) Catalytic activity and life of supported Co catalysts strongly depended on the types of catalytic supports. Co/Al_2O_3 and Co/MgO were more effective catalysts than Co/TiO_2 and Co/MgO. The differences in the catalytic performance according to the supports could be explained by an average size of Co metal crystallites; i.e., Co metal crystallites with sizes of 10−30 nm showed higher activity and longer life for the methane decomposition at 773 K.

(2) Methane decomposition over Co/Al_2O_3 at 773 K produced carbon nanofibers without a hollow structure preferentially, while MWCNT in addition to bamboolike carbon nanotubes were formed during the reaction at 873−973 K. Further increase of the reaction temperatures to 1073 K resulted in the formation of helically coiled carbon nanotubes and bamboolike carbon nanotubes instead of MWCNT.

(3) Co metal particles in the supported Co catalysts were always present at the tip of carbon nanofibers and nanotubes during the methane decomposition at ≤873 K, while they were located in the hollow of carbon nanotubes in addition to the tip of them during the reaction at temperatures ≥973 K.

(4) Co species in the supported Co catalysts were always present as Co metal during the methane decomposition regardless of different reaction temperatures.

References and Notes

(1) Iijima, S. *Nature* **1991**, *354*, 56.
(2) Trans, S. J.; Verschueren, A. R. M.; Dekker, C. *Nature* **1998**, *393*, 49.
(3) Choi, W. B.; Chu, J. U.; Jeong, K. S.; Bae, E. J.; Lee, J. W.; Kim, J. J.; Lee, J. O. *Appl. Phys. Lett.* **2001**, *79*, 3696.

(4) Kong, J.; Yenilmez, E.; Tombler, T. W.; Kim, W.; Liu, L.; Jayanthi, C. S.; Wu, S. Y.; Laughlin, R. B.; Dai, H. *Phys. Rev. Lett.* **2001**, *87*, 106801.
(5) Thess, A.; Lee. R.; Nikolaev, P.; Dai. P.; Petit, P.; Robert, J.; Xu, C.; Lee. Y. H.; Kim, S. G.; Rinzler, A. G.; Colbert, D. T.; Scuseria, G. E.; Tomanek, D.; Fisher, J. E.; Smalley, R. E. *Science* **1996**, *273*, 483.
(6) Ebbesen, T. W.; Ajayan, P. M. *Nature* **1992**, *358*, 220.
(7) Ivanov, V.; Nagy, J. B.; Lambin, P.; Lucas, A.; Zhang, X. B.; Zhang, X. F.; Bernaerts, D.; Van Tendeloo, G.; Amelincks, S.; Van Landuyt, J. *Chem. Phys. Lett.* **1994**, *223*, 329.
(8) Li, W. Z.; Xie, S. S.; Qian, L. X.; Chang, B. S.; Zou, B. S.; Zhou, W. Y.; Zhou, W. Y.; Zhao, R. A.; Wang, G. *Science* **1996**, *274*, 1701.
(9) Ren, Z. F.; Huang, Z. P.; Xu, J. W.; Wang, J. H.; Bush, P.; Siegal, M. P.; Provencio, P. N. *Science* **1998**, *282*, 1105.
(10) Hernadi, K.; Fonseca, A.; Nagy, J. B.; Siska, A.; Kiricsi, I. *Appl. Catal., A* **2000**, *199*, 245.
(11) Soneda, Y.; Duclaux, L.; Béguin, F. *Carbon* **2002**, *40*, 965.
(12) Willems, I.; Kónya, Z.; Colomer, J.-F.; Van Tendeloo, G.; Nagaraju, N.; Fonseca, A.; Nagy, J. B. *Chem. Phys. Lett*. **2001**, *317*, 71.
(13) Wang, P.; Tanabe, E.; Ito, K.; Jia, J.; Morioka, H.; Shishido, T.; Takehira, K. *Appl. Catal., A* **2002**, *231*, 35.
(14) Ishihara, T.; Miyashita, Y.; Iseda, H.; Takita, Y. *Chem. Lett*. **1995**, 93.
(15) Aiello, R.; Fiscus, J. E.; zur Loye, H.-C.; Amiridis, M. D. *Appl. Catal., A* **2000**, *192*, 227.
(16) Choudhary, T. V.; Sivadinarayana, C.; Chusuei, C. C.; Klinghoffer, A.; Goodman, D. W. *J. Catal*. **2001**, *199*, 9.
(17) Otsuka, K.; Kobayashi, K.; Takenaka, S. *Appl. Catal., A* **2001**, *190*, 261.
(18) Takenaka, S.; Kobayashi, S.; Ogihara, H.; Otsuka, K. *J. Catal*. **2003**, *217*, 79.
(19) Piedigrosso, P.; Kónya, Z.; Colomer, J.-F.; Fonseca, A.; Van Tendeloo, G.; Nagy, J. B. *Phys. Chem. Chem. Phys*. **2000**, *2*, 163.
(20) Dai, H.; Rinzler, A. G.; Nikolaev, P.; Thess, A.; Colbert, D. T.; Smalley, R. E. *Phys. Lett*. **1996**, *260*, 471.
(21) Rana, R. K.; Koltypin, Y.; Gadanken, A. *Chem. Phys. Lett*. **2001**, *344*, 256.
(22) Biro, L. P.; Bernardo, C. A.; Tibbetts, G. G.; Lambin, Ph. *Carbon Filaments and Nanotubes: Common Origins, Differing Applications?*; Kluwer Academic Publishers: Boston, MA, 2000.
(23) Zhang, Y.; Smith, K. J. *Catal. Today* **2002**, *77*, 257.
(24) Avdeeva, L. B.; Kochubey, D. I.; Shaikhutdinov, Sh. K. *Appl. Catal., A* **1999**, *177*, 43.
(25) Li. W. Z.; Wen, J. G.; Sennett, M.; Ren, Z. F. *Chem. Phys. Lett*. **2003**, *368*, 299.
(26) Wang, H. Y.; Ruckenstein, E. *Carbon* **2002**, *40*, 1911.
(27) Ankudinov, A.; Ravel, B.; Rehr, J. J.; Conradson, S. D. *Phys. Rev. B* **1998**, *58*, 7565.
(28) Baker, R. T. K. *Carbon* **1989**, *27*, 315.
(29) Rodriguez, N. M. *J. Mater. Res.* **1993**, *8*, 3233.
(30) Pinheiro, J. P.; Gadelle, P. *J. Phys. Chem. Solids* **2001**, *62*, 1023.
(31) Liao, X. Z.; Serquis, A.; Jia, Q. X.; Peterson, D. E.; Zhu, Y. T.; Xu, H. F. *Appl. Phys. Lett*. **2003**, *82*, 2694.
(32) Huffman, G. P.; Shah, N.; Zhao, J.; Huggins, F. E.; Hoost, T. E.; Halvorsen, S.; Goodwin, J. G., Jr. *J. Catal.* **1995**, *151*, 17.
(33) Yoshida, T.; Tanaka, T.; Yoshida, H.; Funabiki, T.; Yoshida, S.; Hasegawa, S. *J. Phys. IV* **1997**, *7*, 1145.
(34) Takenaka, S.; Ogihara, H.; Otsuka, K. *J. Catal*. **2002**, *208*, 54.
(35) Jacobs, G.; Das, T. K.; Patterson, P. M.; Li, J.; Sanchez, L.; Davis, B. H. *Appl. Catal., A* **2003**, *247*, 335.
(36) Jongsomjit, B.; Goodwin, J. G., Jr. *Catal. Today* **2002**, *77*, 191.
(37) Colomer, J.-F.; Stephan, C.; Lefrant, S.; Van Tendeloo, G.; Willems, I.; Kónya, Z.; Fonseca, A.; Laurent, Ch.; Nagy, J. B. *Chem. Phys. Lett.* **2000**, *317*, 83.
(38) Kamalakar, G.; Dennis, W. H.; Hwang, L. *J. Mater. Chem*. **2002**, *12*, 1819.
(39) Kukovitsky, E. F.; L'vov, S. G.; Sainov, N. A. *Chem. Phys. Lett.* **2000**, *317*, 65.
(40) Homma, Y.; Kobayashi, Y.; Ogino, T.; Takagi, D.; Ito, R.; Jung, Y. J.; Ajayan, P. M. *J. Phys. Chem. B* **2003**, *107*, 12161.
(41) Li, Y.; Kim, W.; Zhang, Y.; Rolandi, M.; Wang, D.; Dai, H. *J. Phys. Chem. B* **2001**, *105*, 11424.
(42) Lee, C. H.; Park, J. *Carbon* **2001**, *39*, 1891.
(43) Kim, N. S.; Lee, Y. T.; Park, J.; Ryu, H.; Lee, H. J.; Choi, S. Y.; Choo, J. *J. Phys. Chem. B* **2002**, *106*, 9286.
(44) Kong, J.; Cassell, A. M.; Dai, H. *Chem. Phys. Lett*. **1998**, *292*, 567.